# SYNTHESIS AND CHARACTERIZATION OF $Sb_2O_3$ NANOPARTICLES BY CHEMICAL REDUCTION METHOD

**CHIN HUI SHUN**

**UNIVERSITI SAINS MALAYSIA**

**2012**

# SYNTHESIS AND CHARACTERIZATION OF $Sb_2O_3$ NANOPARTICLES BY CHEMICAL REDUCTION METHOD

**by**

**CHIN HUI SHUN**

**Thesis submitted in fulfillment of the requirements**

**for the Degree of**

**Master of Science**

**March 2012**

## DECLARATION

I declare that this thesis is the result of my own research, that is does not incorporate without acknowledgement any material submitted for a degree or diploma in any university and does not contain any materials previously published, written or produced by another person except where due reference is made in the text.

Signed : ______________________

Candidate's name : Chin Hui Shun

Dated : ______________________

Signed : ______________________

Supervisor's name : Assoc. Prof. Ir. Dr. Cheong Kuan Yew

Dated : ______________________

## ACKNOWLEDGEMENTS

First and foremost, I would like to express my sincere gratitude to my main supervisor, Assoc. Prof. Ir. Dr. Cheong Kuan Yew and co-supervisor Assoc. Prof. Ahmad Badri Ismail for their valuable guidance, advice, knowledge, encouragement and support towards the accomplishment of this research at The School of Materials and Mineral Resources Engineering, USM. In addition, I would like to convey my gratitude to Dr. Khairunisak Abdul Razak for her patience in guiding all the obstacles that I encountered when this research was being carried out. I would also like to acknowledge Assoc. Prof. Dr. Azizan Aziz and Assoc. Prof. Dr. Zainovia Lockman for their comments and inputs throughout this research.

I would like to extend my deepest gratefulness to the Dean of The School of Materials and Mineral Resources Engineering, Prof. Dr. Ahmad Fauzi Mohd Noor and all of the academic, administrative and technical staffs for their continuous assistance and supports during this research, especially Mrs. Fong Lee Lee, Mrs, Haslina, Kak Na, Kak Jamilah, Mr. Azrul, Mr. Zaini, Mr. Rashid, Mr. Zul, Mr. Azam, Mr. Suhaimi and Mr. Farid. Besides, I would like to express my appreciation to technical staffs of The School of Biology, USM for their support on transmission electron microscope (TEM) characterization. I would also like to thank Dr. Mat and Miss Fazira from AMREC, Kulim on helping in high resolution TEM characterization.

I felt indebted and appreciative to USM fellowship, USM Research Universiti Grant (8032035) and USM Short Term Grant (6039038) for the financial support on this research.

Finally, I would like to take this opportunity to express my gratefulness to my family members and friends for their love, encouragement and moral support towards the achievement of this master study. I also sincerely appreciated to those who are directly and indirectly involved in this research.

**CHIN HUI SHUN**

**PGM 0369**

**March 2012**

## TABLE OF CONTENTS

# LIST OF TABLES

# LIST OF FIGURES

## LIST OF ABBREVIATIONS

| | | |
|---|---|---|
| Al | : | Aluminum |
| APCVD | : | Atmospheric Pressure Chemical Vapor Deposition |
| Ar | : | Argon |
| $B_2O_3$ | : | Boron Trioxide |
| Co | : | Cobalt |
| $CO_2$ | : | Carbon Dioxide |
| CTAB | : | Cetyl Trimethyl Ammonium Bromide |
| Cu | : | Copper |
| EG | : | Ethylene Glycol |
| FCC | : | Face-Centered Cubic |
| Fe | : | Iron |
| $H_2O$ | : | Water |
| HILH | : | Hybrid Induction and Laser Heating |
| HRTEM | : | High Resolution Transmission Electron Microscope |
| ICDD | : | International Centre for Diffraction Data |
| $In_2O_3$ | : | Indium Trioxide |
| JCPDS | : | Joint Committee on Powder Diffraction Standard |
| LED | : | Light Emitting Device |
| MOCVD | : | Metal Organic Chemical Vapor Deposition |
| $MoO_3$ | : | Molybdenum Oxide |
| $N_2H_5OH$ | : | Hydrazine |
| NaOH | : | Sodium Hydroxide |
| Ni | : | Nickel |

| | | |
|---|---|---|
| $O_2$ | : | Oxygen |
| Pb: | : | Lead |
| PbO | : | Lead Oxide |
| PET | : | Poly(ethylene terephthalate) |
| PMMA | : | Poly(methyl methacrylate) |
| PVA | : | Polyvinyl Alcohol |
| RoHS | : | Restrictions of Hazardous Substances |
| SAED | : | Selected Area Electron Diffraction |
| Sb | : | Antimony |
| $SbCl_3$ | : | Antimony Trichloride |
| $SbO_2$ | : | Antimony Dioxide |
| $Sb_2O_3$ | : | Antimony Trioxide |
| $Sb_2O_4$ | : | Antimony Tetroxide |
| $Sb_2O_5$ | : | Antimony Pentoxide |
| SDS | : | Sodium Dodecyl Sulfate |
| SEM | : | Scanning Electron Microscope |
| Sn | : | Tin |
| $SnO_2$ | : | Tin Dioxide |
| TEM | : | Transmission Electron Microscope |
| $TiO_2$ | : | Titanium Dioxide |
| UV-vis | : | Ultraviolet-visible |
| XRD | : | X-ray Diffraction |
| ZnO | : | Zinc Oxide |

## LIST OF SYMBOLS

| | | |
|---|---|---|
| $^{o}C$ | | Degree Centigrade |
| α | | Alpha |
| β | : | Beta |
| γ | : | Gamma |
| λ | : | Lambda |
| θ | : | Angle |
| Å | : | Angstrom |
| a | : | Lattice Parameter |
| atm | : | atmosphere |
| Ci | : | curie |
| cos | : | cosinus |
| d | : | Interplanar Spacing |
| g | : | gram |
| $g/cm^3$ | : | gram per cubic centimeter |
| g/mol | : | gram per mole |
| Gy | : | gray |
| h | : | hour |
| K | : | Kelvin |
| kV | : | kilovolt |
| M | : | Molarity |
| mA | : | milliampere |
| mg | : | milligram |
| min | : | minutes |

| | | |
|---|---|---|
| ml | : | milliliter |
| mm | : | millimeter |
| mmol | : | millimoles |
| MPa | : | Megapascal |
| nm | : | nanometer |
| $P^o$ | : | Vapor Pressure |
| Pa | : | Pascal |
| ppm | : | part per million |
| S/cm | : | Siemens per centimeter |
| wt | : | weight |

## LIST OF PUBLICATIONS


1. Chin, H. S., Cheong, K. Y. and Abdul Razak, K. (2010). Review on Oxides of Antimony Nanoparticles: Synthesis, Properties and Applications. Journal of Materials Science, 45, pp. 5993-6008. (Impact Factor: 1.471).

2. Chin, H.S., Cheong, K.Y. and Abdul Razak, K. (2011). Controlled Synthesis of $Sb_2O_3$ Nanoparticles by Chemical Reducing Method in Ethylene Glycol. Journal of Nanoparticle Research, 13, pp. 2807-2818. (Impact Factor: 2.478).

3. Chin, H.S., Cheong, K.Y. and Abdul Razak, K. (2011). Effect of Process Parameters on Size, Shape and Distribution of $Sb_2O_3$ Nanoparticles. Journal of Materials Science, 46, pp. 5129-5139. (Impact Factor: 1.471).

**SINTESIS DAN PENCIRIAN NANOPARTIKEL $Sb_2O_3$ MELALUI KAEDAH PENURUNAN KIMIA**

## ABSTRAK

Nanopartikel antimoni trioksida ($Sb_2O_3$) dengan saiz kurang daripada 100 nm, berbentuk sfera dan taburan yang sekata telah berjaya dihasilkan melalui kaedah penurunan kimia. Antimoni triklorida ($SbCl_3$) telah diturunkan oleh hidrazin dalam kehadiran natrium hidroksida (NaOH) sebagai pemangkin dalam etilena glikol (EG) pada suhu 120 $^{o}$C selama 60 minit. Bagi menghasilkan nanopartikel $Sb_2O_3$ dengan saiz partikel yang kecil (2 - 12 nm), berbentuk sfera dan taburan yang sekata, kesan kepekatan hidrazin ($[N_2H_5OH]/[SbCl_3]$ = 0.75, 5, 10, 20 dan 30), kepekatan NaOH ($[NaOH]/[SbCl_3]$ = 0, 1, 3 dan 5), kepekatan prapenanda ($[SbCl_3]/[N_2H_5OH]$ = 0.05, 0.1, 0.15 dan 0.2), suhu tindak balas (60, 90, 120 dan 150$^{o}$C), masa tindak balas (30, 60, 90 dan 120 minit) dan suhu didih (25, 50, 80 dan 110$^{o}$C) telah dikaji secara sistematik. Microskop penghantaran elektron (TEM), kawasan yang dipilih pola pembelauan elektron (SAED) dan mikroskop elektron resolusi tinggi (HRTEM) telah diaplikasikan untuk mengkaji morfologi dan penghabluran nanopartikel. Pemerhatian menunjukkan bahawa saiz partikel berkurang dan tidak berubah apabila kepekatan hidrazin ($[N_2H_5OH]/[SbCl_3]$) $\geq$ 10. Partikel yang lebih besar telah dihasilkan apabila kepekatan NaOH dan prapenanda, serta suhu dan masa tindak balas dinaikkan. Selanjutnya kajian penghabluran dan fasa nanopartikel telah dibantu oleh pembelauan sinar-X (XRD). XRD menunjukkan bahawa nanopartikel $Sb_2O_3$ adalah dalam fasa kubik. (ICDD file no. 00-043-1071) dengan kekisi jarak 1.68 Å. Walaubagaimanapun, puncak pembelauan $SbCl_3$ telah dikesan apabila hidrazin ditambahkan ke dalam campuran yang belum didih, campuran tersebut mengandungi

kedua-dua $SbCl_3$ dan NaOH dalam EG. Penambahan hidrazin ke dalam campuran yang belum mendidih mempengaruhi mekanisme penurunan $SbCl_3$ dan seterusnya penghasilan nanopartikel $Sb_2O_3$. Analisis ultraungu-nampak (UV-vis) spektrofotometer menunjukkan bahawa penyerapan panjang gelombang maksimum nanopartikel $Sb_2O_3$ telah berlaku dalam linkungan 280 hingga 318 nm. Keputusan kajian menunjukkan partikel yang kecil menyerap pada panjang gelombang UV-vis yang rendah, manakala partikel yang besar menyerap pada panjang gelombang UV-vis yang tinggi. Oleh itu, hubungan antara penyerapan panjang gelombang UV-vis nanopartikel dan saiznya telah ditetapkan.

**SYNTHESIS AND CHARACTERIZATION OF $Sb_2O_3$ NANOPARTICLES BY CHEMICAL REDUCTION METHOD**

## ABSTRACT

Antimony trioxide ($Sb_2O_3$) nanoparticles with particle size less than 100 nm, spherical in shape and well distributed were successfully synthesized by chemical reducing method. Antimony trichloride ($SbCl_3$) was reduced by hydrazine in the presence of sodium hydroxide (NaOH) as catalyst in ethylene glycol (EG) at 120 $^oC$ for 60 minutes. In order to synthesis $Sb_2O_3$ nanoparticles with smaller particle size (2 - 12 nm), spherical in shape and well distribution, effects of hydrazine concentration ($[N_2H_5OH]/[SbCl_3]$ = 0.75, 5, 10, 20 and 30), NaOH concentration ($[NaOH]/[SbCl_3]$ = 0, 1, 3 and 5), precursor concentration ($[SbCl_3]/[N_2H_5OH]$ = 0.05, 0.1, 0.15 and 0.2), reaction temperature (60, 90, 120 and 150$^oC$), reaction time (30, 60, 90 and 120 minutes) and boiling temperature (25, 50, 80 and 110$^oC$) were investigated. Transmission electron microscope (TEM), selected area electron diffraction (SAED) pattern and high resolution electron microscope (HRTEM) were employed to study the morphology and crystallinity of the nanoparticles. It was observed that the particle size decreased and remained constant when concentration of hydrazine ($[N_2H_5OH]/[SbCl_3]$) $\geq$ 10. Increasing the concentration of NaOH and precursor, as well as reaction temperature and reaction time, larger particles were formed. Further study on the crystallinity and phase of the nanoparticles was assisted by X-ray diffraction (XRD). XRD revealed a cubic phase of $Sb_2O_3$ (ICDD file no. 00-043-1071) with lattice spacing of 1.68 Å. However, diffraction peaks of $SbCl_3$ were detected when hydrazine was added into an un-boiled mixture, which consists of both $SbCl_3$ and NaOH in EG. It was found that adding hydrazine to the un-boiled

mixture influenced the mechanism of reduction of $SbCl_3$ and eventually affected the production of $Sb_2O_3$ nanoparticles. From the ultraviolet-visible (UV-vis) spectrophotometer analysis, maximum absorption wavelengths of $Sb_2O_3$ nanoaparticles were occurred from 280 to 318 nm. The results showed that smaller particles were showed lower UV-vis absorption wavelength, while larger particles were showed higher UV-vis absorption wavelength. Therefore, correlation between UV-vis absorption wavelengths of the nanoparticles and their sizes has been established.

# CHAPTER 1

# INTRODUCTION

## 1.1 Introduction

Oxide nanoparticles have received considerable attention over the last few decades for scientific research and technological applications. This is largely related to the exhibition of novel properties by the nanostructured materials when compared with the bulk materials (Iwanaga et al., 1998; Linderoth and Pedersen, 1994). It is well known that the fundamental properties of the nanostructured materials depend strongly on their sizes and shapes (Gleiter, 1989; Salata, 2004). Therefore, researchers have placed much effort into controlling the desired morphologies of these nanostructured materials (Bley and Kauzlarich, 1996; Cao et al., 2001; Han et al., 1997; Jun et al., 2006; Morales and Lieber, 1998; Pan et al., 2001; Rao et al., 2003; Wang and Li, 2006; Xia et al., 2003; Zeng, 2006).

Oxides of antimony (OA) are a key member among all of the other metal oxides from V to VI groups (Huang et al., 2001). Literature (Massalski et al., 1990) reports that there are three phases of well-identified OA, which are antimony trioxide ($Sb_2O_3$), antimony tetroxide ($Sb_2O_4$) and antimony pentoxide ($Sb_2O_5$). The change in Gibbs energy is the key parameter that affects the formation of the desired phase (Khanna, 2002; Samsonov, 1973; Xu et al., 2000; Xu et al., 2004). For instance, $Sb_2O_5$ does not exist above 525$^oC$, only $Sb_2O_3$ and $Sb_2O_4$ are formed. Literature proved that nanoparticles of OA possess excellent properties as compared to bulk OA, for example, a higher refractive index (Nalin et al., 2001; Sahoo and Apparao, 1997), higher abrasive resistance, higher proton conductivity (Dzimitrowicz et al., 1982; Ozawa et al., 1998), excellent mechanical strength (Chang et al., 2009) and higher absorbability (Xie et al., 1999).

In view of the unique properties of OA nanoparticles, a few technological applications have been raised eventually. These applications can be grouped into three fields, namely, chemical, sensing and semiconducting. In the chemical field, OA nanoparticles are useful as a flame retardant synergist using it together with halogenated compounds in plastics, paints, adhesives, sealants, rubbers and textile back coatings (Brebua et al., 2007; Jakab et al., 2003; Jang and Lee, 2000; Laachachi et al., 2004; Pillep et al., 1999; Sato et al., 1998; Xie et al., 2004). In addition, OA nanoparticles also possess a remarkable catalytic property in poly(ethylene terephthalate) (PET) and organic synthesis industries (Duh, 2002; Liu et al., 2001; Matsumura et al., 2006; Nanda et al., 2002; Spengler et al., 2001). Further established uses of OA nanoparticles include as a clarifying agent (Cox et al., 1985; Legouera et al., 2004), opacifier (Zhang et al., 2004), filling agent (Deng et al., 2006), pigments and medicine (Jha and Prasad, 2009b) in the chemical field. In the sensing field, OA nanoparticles are found to possess high proton conductivity properties, making it potentially useful as a promising humidity sensing material (Dzimitrowicz et al., 1982; Ozawa et al., 1998). In the semiconducting field, extremely fine particles (less than 100 nm) of colloidal OA are used as optical materials due to their high refractive index and high abrasive resistance (Nalin et al., 2001; Sahoo and Apparao, 1997).

In general, OA nanoparticles can be synthesized via several methods, which can be classified according to the starting material for synthesizing nanoparticles.

There are three main groups of starting material namely antimony trichloride ($SbCl_3$), antimony (Sb) and slag. For $SbCl_3$ as a starting material, microemulsion (Zhang et al., 2001), solution phase reduction (Ye et al., 2006), hydrothermal (Chen et al., 2008; Edelstein and Cammarata, 1996; Toraya et al., 1983; Zhang and Gao, 2004), γ-ray radiation-oxidization (Liu et al., 1996; Liu et al., 1997) and biosynthesis (Jha and Prasad, 2009a; Jha and Prasad, 2009b) methods have been used. On the other hand, pure Sb is used as a precursor to synthesize OA nanoparticles via a hybrid induction and laser heating (HILH) method (Siegel, 1994; Tigau et al., 2004; Wu et al., 2000a; Wu et al., 2000b; Xie et al., 1999; Zeng et al., 2004a; Zeng et al., 2004b), as well as thermal oxidation method (Xu et al., 2007). Furthermore, vacuum evaporation (Qiu and Zhang, 2006) method by using slag as a starting material has been reported as a potential solution for producing OA nanoparticles. However, there are some limitations associated with these methods mainly due to the high temperature and high pressure for hydrothermal synthesis (Chen et al., 2008) and complicated techniques for the γ-ray radiation-oxidization route (Liu et al., 1997). Consequently, chemical method is appeared to be the most successful method in synthesizing of $Sb_2O_3$ nanoparticles. This is owing to its capability to synthesize $Sb_2O_3$ nanoparticles in the simplest, shortest time (~ 1 h) and least expensive (Chen et al., 2008; Chin et al., 2010b; Jha and Prasad, 2009b; Liu et al., 1997; Qiu and Zhang, 2006; Xu et al., 2007; Zeng et al., 2004a; Zeng et al., 2004b), which are favorable in the large scale industrial production.

## 1.2 Problem Statement

Recently, progressive development of nanotechnology has triggered the synthesis of particles in nanometer scale. Nanoparticles possess novel electronic, chemical, mechanical, optical, sensing and catalytic properties, which are different from those bulk materials due to their high surface-to-volume ratio (Wang et al., 2009; Ye et al., 2006). These properties find applications in the field of flame retardant synergist, catalyst, optical material, sensor, electronic and optoelectronic devices (Duh, 2002; Dzimitrowicz et al., 1982; Feng et al., 2007; Laachachi et al., 2004; Nalin et al., 2001; Ozawa et al., 1998; Sahoo and Apparao, 1997; Xie et al., 2004). Nanoparticles are commonly incorporated in polymers acting as a flame retardant compound to prevent burning of the polymers. There are some commonly used flame retardants synergist such as $Sb_2O_3$, aluminum trihydrate and magnesium hydroxide (Feng et al., 2007). Among those reported candidates, $Sb_2O_3$ is a well known flame retardant synergist, which is applied in plastics and rubber. However, larger particle size and lower mechanical properties have limited their applications (Feng et al., 2007). Thus, most efforts have been focused to synthesize $Sb_2O_3$ nanoparticles in the smallest size, with spherical shape and well distribution.

Up to now, $Sb_2O_3$ nanoparticles have been successfully synthesized in polyhedral shape with particle size less than 200 nm by chemical method (Zhang et al., 2001). This method enables $Sb_2O_3$ to be synthesized in nanoparticles form at the shortest time (~ 1 h), lowest cost and simplest route, if compared to other reported methods (Chen et al., 2008; Chin et al., 2010b; Jha and Prasad, 2009b; Liu et al., 1997; Qiu and Zhang, 2006; Xu et al., 2007; Zeng et al., 2004a; Zeng et al., 2004b). In this method, polyvinyl alcohol (PVA) and sodium hydroxide (NaOH) were used to synthesize the $Sb_2O_3$ nanoparticles. However, larger particle size with polyhedral shape has limitation in their application as flame retardant synergist. To overcome this issue, the chemical method has been modified into chemical reduction method, where hydrazine ($N_2H_5OH$) acting as a reducing agent and ethylene glycol (EG) acting as a protective agent solvent were introduced. It was reported that this chemical reducing method is able to synthesize nanoparticles of nickel (Ni) with mean particle size of 9.2 nm in spherical shape and the size is distributed uniformly (Wu and Chen, 2003). In the system of cobalt (Co), particle size ranges from 4 to 13 nm in spherical shape with well distribution were successfully synthesized by reduction of ion $Co^{2+}$ with hydrazine in EG (Balela, 2008).

In chemical reduction method, there are a few process parameters that contribute to the particle size, shape and distribution of nanoparticles. Some of the reported parameters are concentration of hydrazine, NaOH and precursor, reaction temperature and reaction time (Balela, 2008; Chin et al., 2010a; Kim and Kim, 2003; Lee et al., 2007; Pattabi and Saraswathi, 2007; Segets et al., 2009; Yang et al., 2007; Zhang et al., 2008). It was found that increasing reaction temperature (Segets et al., 2009; Zhang et al., 2008) , reaction time (Kim and Kim, 2003; Lee et al., 2007; Yang et al., 2007) and concentration of precursor (Balela, 2008; Pattabi and Saraswathi, 2007) caused greater effect on the growth rather than on the nucleation of other systems, where particle size increased with the increase of reaction temperature, reaction time and concentration of precursor, respectively. However, there is no report on the aforementioned process parameters on the synthesis of $Sb_2O_3$ nanoparticles via chemical reduction method. Therefore, the effects of concentration of hydrazine, NaOH and precursor, reaction temperature, reaction time and boiling temperature have been systematically investigated in this study, aiming to produce $Sb_2O_3$ nanoparticles with smallest diameter, spherical in shape and well distributed.

## 1.3 Objectives of the Research

The main purpose of this research is to produce $Sb_2O_3$ nanoparticles by chemical reduction method. The objectives are as follows:

(a) To synthesis well-distributed $Sb_2O_3$ nanoparticles with smaller particle size (less than 100 nm) and spherical in shape.

(b) To investigate the effect of hydrazine, NaOH and precursor concentration, as well as reaction temperature, reaction time and boiling temperature on the particle size, shape and distribution of $Sb_2O_3$ nanoparticles.

(c) To study the morphologies, phases, crystal structures and ultraviolet-visible (UV-vis) absorption spectra of $Sb_2O_3$ nanoparticles.

## 1.4 Scope of the Research

In this work, $Sb_2O_3$ nanoparticles were synthesized in the presence of protective agent solvent (EG), through the reaction of precursor ($SbCl_3$), reducing agent (hydrazine) and catalyst/pH adjustor (NaOH). The mixture was stirred for 60 min at 120$^{o}$C until white precipitates are obtained. The precipitates were filtered by washing several times with distilled water and ethanol. After that, the precipitates were dried at 100$^{o}$C for 60 min. The effects of concentration of hydrazine, NaOH and precursor, reaction temperature, reaction time and boiling temperature on the size, shape and distribution of the $Sb_2O_3$ nanoparticles were investigated. The morphologies were examined by using a transmission electron microscope (TEM). Crystalline phases were characterized by X-ray diffraction (XRD), selected area electron diffraction (SAED) and high resolution TEM (HRTEM). Ultraviolet-visible (UV-vis) absorption spectra of nanoparticles were analyzed by UV-vis spectrophotometer.

## 1.5 Organization of the Thesis

There are total of five chapters in this thesis. The first chapter briefly introduces the background and problem statement, research objectives and also scope of the research. Literature review of the research is elucidated in the second chapter. Chapter three presents the materials and methodology of the research. Next, the fourth chapter discusses the results and discussion of the research. At last, conclusions and recommendations for future research are explained in the fifth chapter.

# CHAPTER 2

# LITERATURE REVIEW

## 2.1 Introduction

In this chapter, properties of the different phases of OA (bulk), as well as a comparison of properties between nanoparticles and bulk OA are reviewed. Various types of methods to synthesis $Sb_2O_3$ nanoparticles, its outcomes and challenges faced during synthesizing, are being explained. With the excellent properties being demonstrated, some of the potential applications of OA nanoparticles have been discussed.

## 2.2 Phases and Properties of Oxides of Antimony (OA)

### 2.2.1 Phases

Massalski et al. (1990) identified three main phases of OA, namely, $Sb_2O_3$, $Sb_2O_4$ and $Sb_2O_5$. Typically, $Sb_2O_3$ has two crystalline modifications, cubic polymorph (senarmontite stable phase) and orthorhombic polymorph (valentinite metastable phase) (Remy, 1956). It was found that orthorhombic polymorph can be transformed into cubic polymorph at 490-530$^{o}$C (Whitten et al., 2004). In addition, senarmontite exists as a low temperature α-phase and valentinite as a high temperature β-phase (Svensson, 1974; Svensson, 1975). The differences of both polymorphs lie in their different physical and chemical properties.

Formation of the three phases is controlled by the reaction of both thermodynamic and kinetic activities of the metal and oxides, which is related directly to the change in Gibbs energy (Khanna, 2002; Samsonov, 1973; Xu et al., 2000; Xu et al., 2004). For example, $Sb_2O_5$ does not form above 525°C, and thus, only both $Sb_2O_3$ and $SbO_2$ ($Sb_2O_4$) exist. According to the theory of oxidation, a multilayer scale will form on the metal when more than one type of oxide coexists with the metal in the system (Khanna, 2002). The multilayer scale described by varying oxygen content, from metal-rich oxides (low oxygen equilibrium pressure) to oxygen-rich oxides (high oxygen equilibrium pressure) is shown in Figure 2.1a. At the same time, $SbO_2$ will be further oxidized in air to form a much more stable oxide, which is $Sb_2O_3$ (Figure 2.1b).

On the other hand, $Sb_2O_5$ can be prepared by oxidizing antimony with concentrated nitric acid and the prepared $Sb_2O_5$ is normally in hydrated state (Remy, 1956). $Sb_2O_4$ is a compound of $Sb_2O_3$ and $Sb_2O_5$, where it contains mixed valence of Sb(III) and Sb(V). The two stable modifications of $Sb_2O_4$ are the room temperature orthorhombic α-phase (cervantite) and high temperature monoclinic β-phase (Amador et al., 1988). Hence, $Sb_2O_4$ can be obtained by two possible routes, either heating $Sb_2O_3$ in air or prolonged heating hydrated $Sb_2O_5$ at 800°C, as shown in Eq. (2.1) and Eq. (2.2) (Remy, 1956).

$$Sb_2O_3 + 0.5O_2 \rightarrow Sb_2O_4 \quad \Delta H = -187 \text{ kJ/mol} \tag{2.1}$$

$$Sb_2O_5 \rightarrow Sb_2O_4 + 0.5O_2 \quad \Delta H = -64 \text{ kJ/mol} \tag{2.2}$$

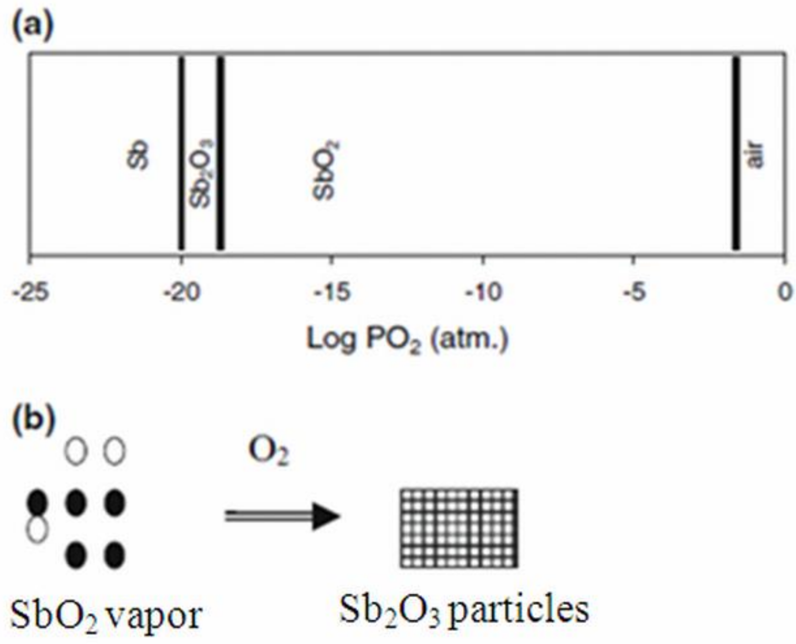


Figure 2.1**:** Illustration of the formation of (a) multilayer scale on metal Sb and (b) stable $Sb_2O_3$ particles (Xu et al., 2007).

### 2.2.2 Properties

Table 2.1 (Remy, 1956) presents various properties of the three phases of OA ($Sb_2O_3$, $Sb_2O_4$ and $Sb_2O_5$) in the bulk form. In general, OA appears as a solid or powder ranging from white to yellow in color. These are the white solid ($Sb_2O_3$), white or yellow solid ($Sb_2O_4$) and yellow solid ($Sb_2O_5$). The densities of OA phases will sequence from $Sb_2O_3$, $Sb_2O_4$ and $Sb_2O_5$ are 5.2, 6.64 and 3.78 g/cm$^3$, respectively. $Sb_2O_3$ melts at 636$^o$C and boils at 1425$^o$C, in which the melting point is higher than that of $Sb_2O_5$ which is 380$^o$C. Based on the solubility in water only $Sb_2O_5$ is reported to be very soluble when compared to both $Sb_2O_3$ and $Sb_2O_4$, which are insoluble in water. $Sb_2O_3$ exists in two forms, cubic and orthorhombic. When heating is carried out above 570$^o$C, orthorhombic $Sb_2O_3$ is formed and cubic $Sb_2O_3$ will be formed when heating is conducted below 570$^o$C.

Researchers reported that OA nanoparticles possess novel or excellent properties compared to bulk OA (Gleiter, 1989; Iwanaga et al., 1998; Linderoth and Pedersen, 1994), some of the studied properties are summarized in Table 2.2. By definition, nanoparticles have sizes less than 100 nm with a much bigger surface area as compared to bulk materials. In flame retardant manufacturing, impact strength and translucent are two main properties that affect the quality of the products (Xie et al., 2004). The bulk OA contributes to higher losses in translucency, which restricts the range of available color choices. It is because higher colorant loading is required to counterbalance the tinting effect of OA. Using nanoparticles of OA, colorant loadings can be abridged one-third to one-half of the normal quantity utilized. Thus, it helps in reducing the manufacturing cost and improves the properties or quality of the products. Consequently, the mechanical properties (impact strength and tensile strength) of OA nanoparticles are improved (Chang et al., 2009). In conjunction with the bigger surface area of OA nanoparticles, it has strong absorption property (Xie et al., 1999) for metallic impurities, thus enhancing the performance of the epoxy in electronic applications. Furthermore, Lie et al. (2008) reported that OA nanoparticles behave stable superhydrophobic properties with a small sliding angle ($5^o$) when compared to bulk OA, where this will expand the existing applications of OA.

Table 2.1: Summary properties of three phases of OA in bulk (Remy, 1956).

| Properties | $Sb_2O_3$ | $Sb_2O_4$ | $Sb_2O_5$ |
|---|---|---|---|
| Appearance | White solid | White or yellow solid | Yellow solid |
| Molecular weight (g/mol) | 291.52 | 307.52 | 323.52 |
| Density (g/cm$^3$) | 5.2 | 6.64 | 3.78 |
| Melting point ($^oC$) | 656 | N/A | 380 |
| Boiling point ($^oC$) | 1425 | N/A | N/A |
| Crystal structure | Cubic (< 570$^oC$)<br>Orthorhombic (> 570$^oC$) | Orthorhombic<br>Monoclinic | N/A |
| Solubility in water | Insoluble | Insoluble | Very slightly soluble |

Table 2.2: Comparison properties of both bulk and nanoparticles of OA (Chang et al., 2009; Dzimitrowicz et al., 1982; Liu et al., 2008; Mostashari and Baie, 2008; Nalin et al., 2001; Nyffenegger et al., 1998; Ozawa et al., 1998; Sahoo and Apparao, 1997; Tigau et al., 2005; Xie et al., 1999; Xie et al., 2004).

| Properties | OA-bulk | OA-nanoparticles |
|---|---|---|
| Particle size | > 100 nm | < 100 nm |
| Translucent | Maximum loss | Minimum loss |
| Colorant loading | Higher | Reduced half of bulk |
| Impact strength | Lower | Higher |
| Tensile strength | Lower (< 4.05 MPa) | Higher (4.05 - 9.35 MPa) |
| Absorbability | Weak | Strong |
| Superhydrophobic | Unstable<br>(sliding angle > 5$^o$) | Stable<br>(sliding angle < 5$^o$) |
| Refractive index | Lower (< 2) | Higher (> 2) |
| Abrasive resistance | Lower | Higher |
| UV vis absorbance | Lower<br>(< 0.3 a.u of absorbance) | Higher<br>(> 0.3 a.u of absorbance) |
| Proton conductivity | Lower<br>(< 2.89 x 10$^{-3}$ S/cm) | Higher<br>(2.89 x 10$^{-3}$ S/cm) |

By investigating the photoluminescence properties of OA nanoparticles, it indicated strong emission band at 374 nm with an optical bandgap $E_g$ = 3.3 eV, which are located in the near-ultraviolet (UV) region (Deng et al., 2006). Besides, the quantum effect of the OA nanoparticles will enhance the UV absorbance of OA (Nyffenegger et al., 1998). Therefore, it could be used in a UV light emitting device (LED) and in solar cell technology (Tigau et al., 2005). Moreover, Chen et al. (2008) claimed that OA nanoparticles exhibited a significant red shift (2.32 - 3.33 eV) in emission band, as compared to bulk OA (4.31 eV), which suggested potential usage in optoelectronic devices. On the other hand, OA nanoparticles-based glasses exhibited extended infrared transmission, higher refractive index and higher abrasive resistance, as compared to borosilicates (Nalin et al., 2001; Sahoo and Apparao, 1997). For instance, orthorhombic phase of OA nanoparticles is a main component in $Sb_2O_3$-$B_2O_3$ glasses, where it helps in improving the non-linear optical properties (Terashima et al., 1996).

In term of sensing perspective, OA nanoparticles possess both humidity and gas-sensing properties. Owing to its higher proton conductivity properties when compared to bulk form, OA nanoparticles are found to be a potential humidity sensor. Ozawa et al. and Dzimitrowicz et al. (1982; 1998) investigated that the electrical conductivity of OA increases from $1.69 \times 10^{-5}$ to $2.89 \times 10^{-3}$ S/cm as the relative humidity altered from 11 to 85 %. In the case of gas-sensing properties, OA-based gas sensor prepared by metal organic chemical vapor deposition (MOCVD) method, indicated a great response to methane gas and fully recovered once the removal of the gas (Binions et al., 2006). By preparing via screen printing method, OA-based gas sensor exhibited fast response to 100 ppm of ethanol at operating temperature of 500$^oC$. Meanwhile, OA-based gas sensor also behaved quick recovery, when changing from ethanol flow to clean air flow (Binions et al., 2006).

## 2.3 Synthesis Methods

There are few methods that have been reported to synthesis OA nanoparticles, which can be categorized into three groups according to the starting material during synthesis. The three groups are: $SbCl_3$, Sb, and slag as starting materials. The details of the synthesis methods are reviewed in the subsequent paragraphs and are summarized in Table 2.3.

### 2.3.1 Starting Material: Antimony Trichloride ($SbCl_3$)

#### 2.3.1.1 Microemulsion

Zhang et al. (2001) reported the synthesis of OA nanoparticles via microemulsion method using PVA. There are two main functions of PVA in this method: one is to prevent agglomeration of the formed nanoparticles and the other is to form a spherical reactor. In this method, a 228 mg of $SbCl_3$ as a starting material was dissolved into 100 ml of hydrochloride acid solution (1 M). After dissolving, 3 g of PVA was added. Then the mixture was ultrasonically vibrated for 15 min, followed by dropping 12 ml of NaOH into the mixture slowly until the mixture turns to transparent pale yellow color. In order to bring about a more intense color, the solution was refluxed for 1 h. During refluxing, the solvent was evaporated at 80$^oC$ in a reduced atmosphere. The final product, which was in the form of dry powders were obtained by heating the solvent at 350$^oC$ under an ambient atmosphere for 1 h.

Table 2.3: Summary of varies synthesis methods of $Sb_2O_3$ nanoparticles.

| Starting material | Synthesis methods | Size (nm) | Size distribution | Shape | Structure | Limitations | References |
|---|---|---|---|---|---|---|---|
| $SbCl_3$ | Microemulsion | 10 - 80 | Random | Polyhedral | Cubic (FCC) | Required heating to 350$^{o}$C to get powder | (Zhang et al., 2001) |
| | Solution phase reduction | 17 $\pm$1 | Uniform | Spherical | Cubic (FCC) | Required stirring for 24 h | (Ye et al., 2006) |
| | Hydrothermal | ~ 500 | N/A | Spherical | Cubic (FCC) | Required heating for 12 h | (Chen et al., 2008) |
| | | < 100 | Uniform | N/A | Orthorho mbic | | |
| | γ-ray radiation-oxidization | 8 - 48 | N/A | Spherical | Cubic (FCC) | Complex techniques | (Liu et al., 1997) |
| | Biosynthesis | 2 - 10 | Uniform | Spherical | Cubic (FCC) | Longer processing time (~ 6 days) | (Jha and Prasad, 2009a; Jha and Prasad, 2009b) |
| Sb | Hybrid induction and laser heating (HILH) | 80 | Uniform | Spherical | Cubic (FCC) | Obtained mixture of Sb and $Sb_2O_3$ nanoparticles<br><br>Expensive experimental | (Zeng et al., 2004a; Zeng et al., 2004b) |

| | | | | | | | |
|---|---|---|---|---|---|---|---|
| | | | | | | setup | |
| | Thermal oxidation | 10 - 100 | Random | Polyhedral | Cubic (FCC) | Required minimum deposition time for 4 h | (Xu et al., 2007) |
| Slag | Vacuum evaporation | < 100 | Uniform | Spherical | Cubic (FCC) | High temperature (893 K) and high pressure (250 Pa) | (Qiu and Zhang, 2006) |

TEM analysis revealed that the nanoparticles are in polyhedral shape while their sizes range from 10 to 80 nm (Figure 2.2). The difference in shape and size of the nanoparticles are mainly due to the growth process of the nanoparticles, in which they begin to grow in a different stages and periods. Furthermore, the SAED pattern inserted at right bottom corner of Figure 2.2 shows that the nanoparticles consist of many reflection rings, which means the structure of nanoparticles are polycrystalline. Table 2.4 shows the comparison of experimental planar spacing and the standard data from Joint Committee on Powder Diffraction Standard (JCPDS) card (43-1071). It is observed that both planar spacing are well consistent with cubic $Sb_2O_3$, which has the space group *Fd*3*m*. Large-angle tilting diffraction patterns on a larger antimony oxide nanoparticle (~ 60 nm) as shown in Figure 2.3, show that the crystal structure of nanoparticles is face-centered cubic (FCC).

Table 2.4: Comparison between the experimental planar spacing and the standard data from JCPDS card (Zhang et al., 2001).

| Radium (mm) | $d_{exp}$ | $d_{cal}$ | (hkl) | Relative intensity |
|---|---|---|---|---|
| $R1 = 1.98$ | 6.35 | 6.439 | (111) | 15 |
| $R2 = 3.90$ | 3.17 | 3.219 | (222) | 100 |
| $R3 = 4.50$ | 2.75 | 2.788 | (400) | 33 |
| $R4 = 4.87$ | 2.54 | 2.558 | (331) | 8 |
| $R5 = 5.60$ | 2.21 | 2.2765 | (422) | 1 |
| $R6 = 6.40$ | 1.93 | 1.9714 | (440) | 33 |
| $R7 = 7.50$ | 1.65 | 1.6812 | (622) | 30 |

$d_{cal}$ from the JCPDS card

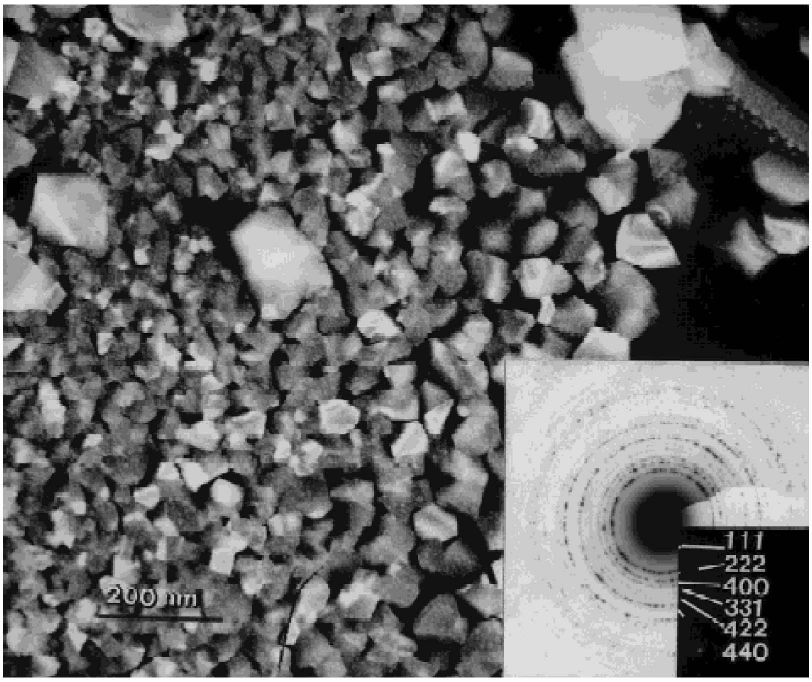


Figure 2.2: TEM micrograph showing the morphology of antimony oxide nanoparticles and the corresponding SAED is inserted at the right bottom corner (Zhang et al., 2001).

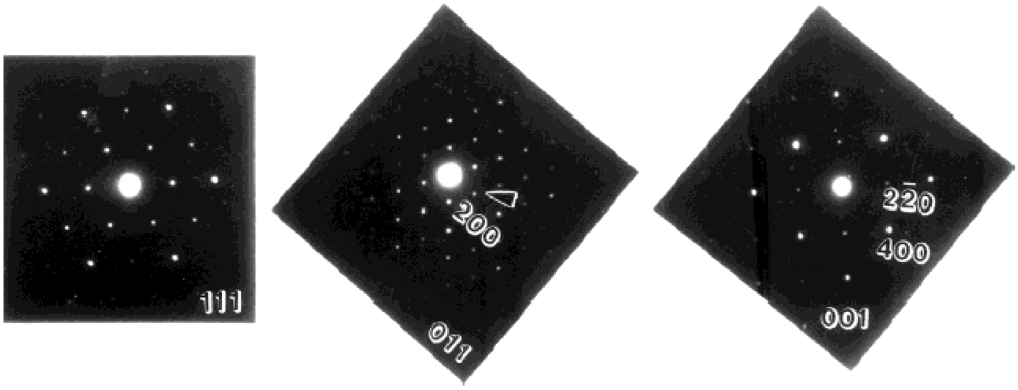


Figure 2.3: Large-angle tilting diffraction patterns on a larger antimony oxide particle (~ 60 nm) (Zhang et al., 2001).

In summary, this method is a simple way to synthesis of OA nanoparticles using PVA through a reaction between $SbCl_3$ and NaOH (Zhang et al., 2001). The achieved sizes of the nanoparticles are range from 10 to 80 nm in polyhedral forms. SAED revealed that the nanoparticles are polycrystalline in structure. From characterization, it can be concluded that the nanoparticles are mainly $Sb_2O_3$ cubic (FCC) structure.

**2.3.1.2 Solution Phase Reduction**

Ye et al. (2006) on the other hand, reported the successful synthesis of $Sb_2O_3$ nanoparticles using Cetyl Trimethyl Ammonium Bromide (CTAB) as a soft template and employing $Sb(OH)^-_4$ as an inorganic precursor (formed by controlling pH of the $SbCl_3$ solution to value of 14 (Xiang et al., 2000). In this solution phase reduction method, 0.15 mmol (or even less) of CTAB was added into a 100 ml solution of 0.01 M $SbCl_3$ under constant stirring for 2 h until CTAB is dissolved fully. In order to reach a pH value of 14, 1 M of NaOH solution was added dropwise to the above mixture. Subsequently, the resulting solution was stirred for 24 h at room temperature, followed by putting it into an oven at $60^oC$ for 4 h. After heating was completed, the light brown precipitate was centrifuged and washed multiple times using ethanol and distilled water. Then, the precipitate was dried under vacuum at room temperature gradually.

In Figure 2.4, $Sb_2O_3$ nanoparticles in spherical shape with a narrow size distribution or having a diameter of 17 $\pm$ 1 nm were observed under the scanning electron microscope (SEM). These morphologies can be explained in terms of the CTAB concentration, where lower CTAB concentration favors the lowest order phase such as the spherical shape structure and higher CTAB concentration contributes to a higher ordered phase such as nanowires and nanoribbons (Leontidis et al., 1999; Pileni, 2001; Pinna et al., 2001; Wang et al., 2001). The electrostatic interaction between $Sb(OH)^{-}_{4}$ anions and CTAB cations formed $CTA^{+}$ - $Sb(OH)^{-}_{4}$ ion pairs (Cao et al., 2003). The lower concentrations of $CTA^{+}$ cations caused the necessary charge compensating anions to decrease and led the system to find its minimum energy configuration by adopting the spherical structure (Biz and Occelli, 1998). Therefore, $Sb_2O_3$ nanoparticles were formed after the subsequent thermal treatment. In order to understand the crystal structure and phase of the nanoparticles, XRD was carried out. From the diffraction peak in the XRD spectrum as shown in Figure 2.5, it was concluded that the $Sb_2O_3$ nanoparticles were in cubic phase according to the literature (JCPDS card 42-1466). Meanwhile, the XRD results also indicated that no other phases were detected from the spectrum.

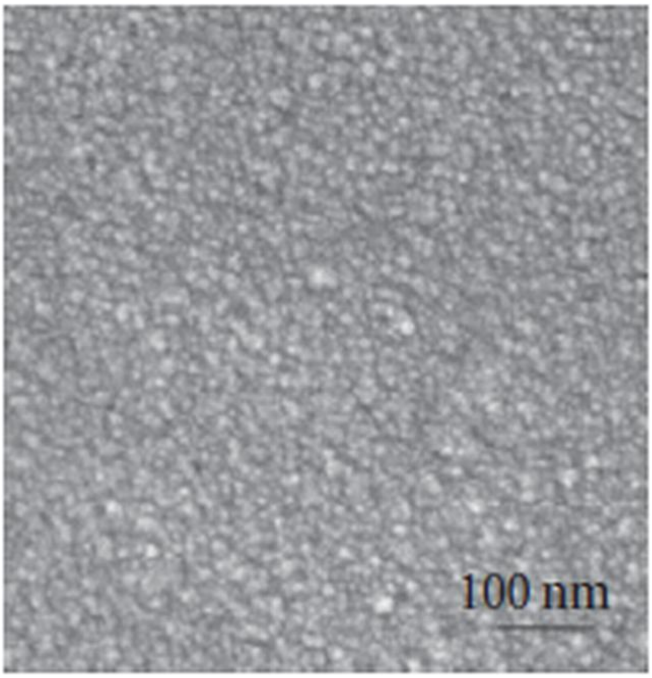


Figure 2.4: SEM image of $Sb_2O_3$ nanoparticles obtained by CTAB (Ye et al., 2006).

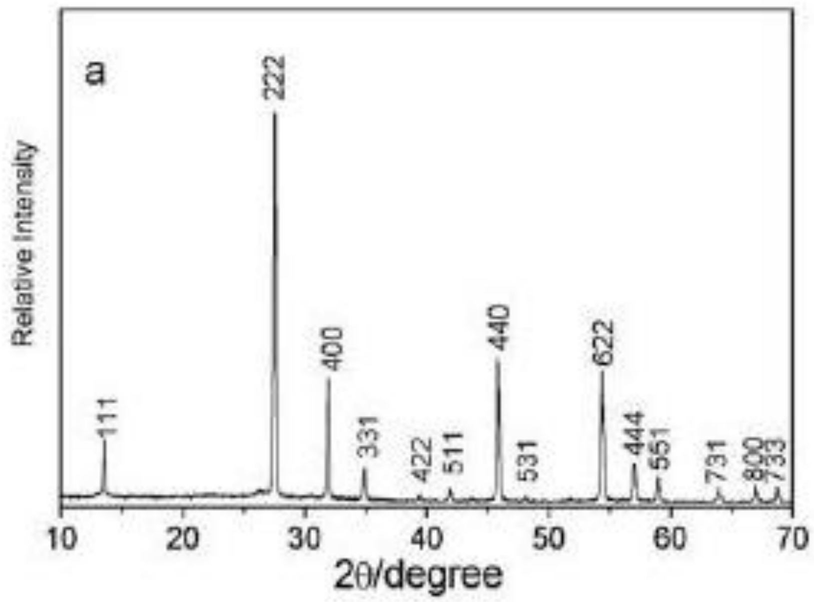


Figure 2.5: XRD spectrum of $Sb_2O_3$ cubic phase (Chen et al., 2008).

In conclusion, cubic phase of $Sb_2O_3$ nanoparticles with narrow distribution (17 ± 1 nm) and spherical in shape were successfully synthesized by adopting CTAB as a soft template. The advantages of this method are easy handling, relatively low cost and large-scale production. The control of the CTAB concentration to synthesize $Sb_2O_3$ nanostructures is beneficial in flame retardant and catalyst applications. Furthermore, this facile synthesis method could be explored to synthesize other nanostructures, such as $SnO_2$ (Ye et al., 2004).

**2.3.1.3 Hydrothermal**

Chen et al. (2008) studied the preparation of antimony oxide nanoparticles via a hydrothermal method. Both cubic and orthorhombic phase of $Sb_2O_3$ nanoparticles can be obtained by varying the solvent composition, such as EG - water ($H_2O$) and toluene - $H_2O$. Besides, the control of pH value is an important parameter to determine the morphologies of the nanostructures. In this method, 2 mmol of $SbCl_3$ was dissolved in 20 ml of EG solution under vigorous stirring to form a transparent solution. Subsequently, 20 ml of distilled water was added to the above solution to obtain a lacteous colloid. Then, the resulting mixture was stirred for 15 min and 6 M of NaOH solution was added to adjust the pH value in the range of 8 - 9. The whole solution was stirred for another 20 min before being transferred into a 100 ml Teflon-lined stainless steel autoclave. The autoclave was sealed and kept at 120$^{o}$C. After 12 h, the resulting white product was centrifuged and washed several times with distilled water and ethanol, and then vacuum dried at 60$^{o}$C for 6 h. In order to investigate the effect of solvent composition on the phase formation of $Sb_2O_3$ nanoparticles, the same procedures were repeated by replacing EG solution with toluene solution.

XRD was used to observe the phase presence, crystallinity and purity of the samples which were synthesized in both EG - $H_2O$ and toluene - $H_2O$ at 120$^{o}$C for 12 h. The reflection spectrums in both Figure 2.5 and 2.6 could be directly indexed as cubic $Sb_2O_3$ (JCPDS card 5-534) and orthorhombic $Sb_2O_3$ (JCPDS card 11-689), respectively. Furthermore, no other phases existed in both spectrums, which strongly suggested the formation of pure cubic $Sb_2O_3$ and orthorhombic $Sb_2O_3$ in pH 8 - 9. From the XRD spectrums, solvent composition is critical to control the phase of $Sb_2O_3$. TEM image in Figure 2.7 displays the morphology of sub-micronmeter (~ 500 nm) cubic (FCC) $Sb_2O_3$ particles which are almost spherical shape. Figure 2.8 shows the corresponding HRTEM image obtained at the edge of the $Sb_2O_3$ nanoparticle, broad lattice spaces of 0.32 and 0.64 nm are found and matched the (222) and (111) planes, which are indicated in the inserted SAED image. Tiny orthorhombic $Sb_2O_3$ nanoparticles (< 100 nm) are revealed in Figure 2.9 which were obtained at pH 8 - 9 in toluene - $H_2O$. From the nanostructure synthesis perspective, EG is well known to support two functions: one as a reducing agent to prepare metal or alloy nanoparticles and the other one as coordination agent or temporary ligand in the synthesis of $SnO_2$, $TiO_2$, PbO and $In_2O_3$ nanoparticles (Kempf et al., 1996; Scott et al., 2003; Wang et al., 2003). The chelating ligand EG binds strongly to metal to form a more stable complex, whereas the nonchelating ligand toluene binds weakly to the metal. The different capability in its ability to bind with metal contributed to the formation of different phases of $Sb_2O_3$ nanoparticles. Thus, cubic $Sb_2O_3$ and orthorhombic $Sb_2O_3$ can be synthesized by choosing a proper solvent composition.

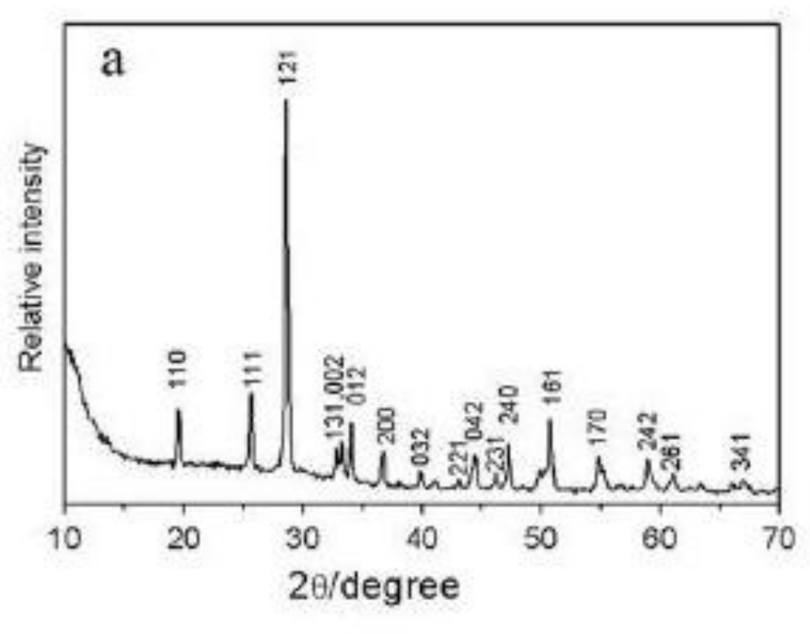


Figure 2.6: XRD spectrum of the sample obtained in toluene - $H_2O$ (Chen et al., 2008).

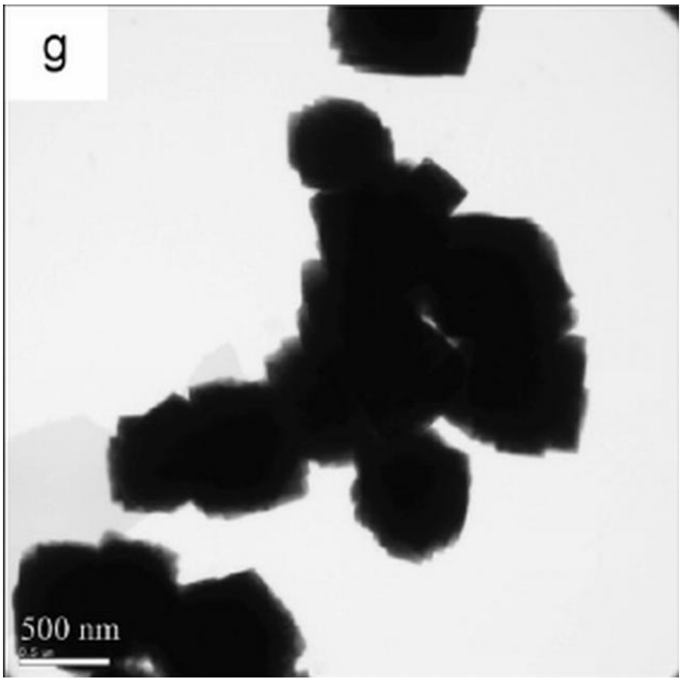


Figure 2.7: TEM image of sample obtained in EG - $H_2O$ (Chen et al., 2008).

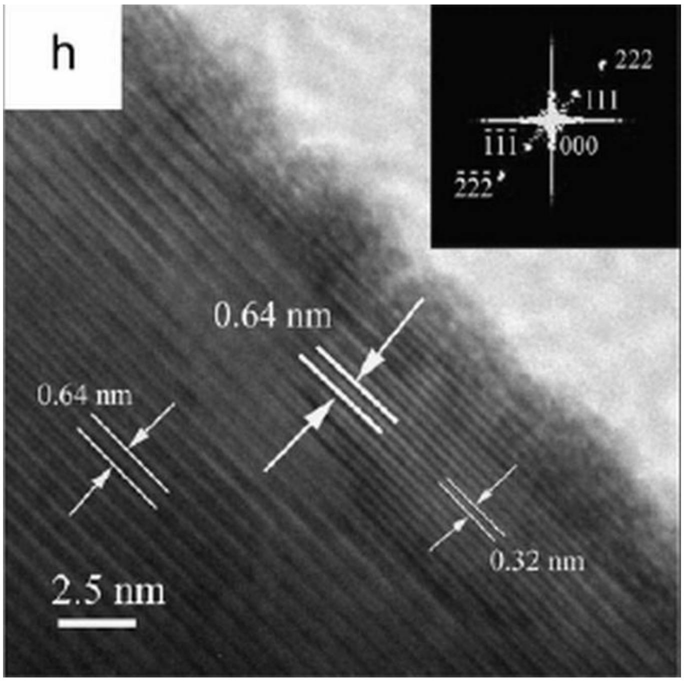


Figure 2.8: HRTEM SAED image of sample obtained in EG - $H_2O$ (Chen et al., 2008).

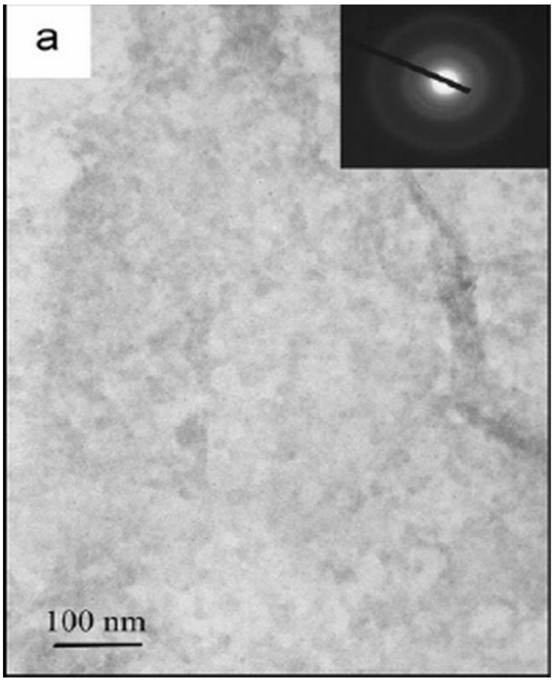


Figure 2.9: TEM image of sample obtained in toluene - $H_2O$ (Chen et al., 2008).

In summary (Table 2.5), the sizes and phases of nanoparticles in this study were strongly affected by the solvent composition and pH of the reaction mixture (Chen et al., 2008). In this content, $Sb_2O_3$ nanoparticles were synthesized at pH 8 - 9 in both EG - $H_2O$ and toluene - $H_2O$. EG - $H_2O$ favored the formation of cubic $Sb_2O_3$ nanoparticles whereas toluene - $H_2O$ favored the formation of orthorhombic $Sb_2O_3$ nanoparticles.

Table 2.5: Summary of $Sb_2O_3$ particles obtained at 120$^oC$ for 12 h in mixed solvents (Chen et al., 2008).

| Product | pH | Solvent composition | Phase | Size (nm) |
|---|---|---|---|---|
| $Sb_2O_3$ | 8-9 | EG - $H_2O$ | Cubic (FCC) | ~ 500 |
| | | Toluene - $H_2O$ | Orthorhombic | < 100 |